ATLAS PUB Note

ATL-PHYS-PUB-2018-021

October 24, 2018

ATLAS sensitivity to top squark pair production at the HL-LHC

The ATLAS Collaboration

This document summarises the expected sensitivity of the ATLAS detector to top squarks with 3 ab^{-1} of $\sqrt{s}$ = 14 TeV proton-proton collisions collected at the HL-LHC. The top squarks are pair produced and assumed to decay into a top quark and a neutralino. Prompt leptons are vetoed in the final state, which is only composed by jets and missing transverse momentum. A 5σ discovery (95% CL exclusion) can be obtained for top squark masses up to 1.25 (1.7) TeV and small neutralino masses, assuming realistic projections of the systematic uncertainties. If the top squark mass equals the sum of the top quark and neutralino masses, then a 5σ discovery (95% CL exclusion) can be achieved up to about 650 (850) GeV.

ATL-PHYS-PUB-2018-021
25 October 2018

1 Introduction

The aim of this note is to assess the ATLAS sensitivity to top squark (stop in the following) pair production using the dataset expected to be collected by the upgraded detector during the Large Hadron Collider (LHC) high luminosity data-taking (HL-LHC in the following). The stops are the scalar supersymmetric [1–6] partners of the top quark fermionic degrees of freedom: for each of the two top chirality eigenstates t_L, t_R the existence of partner scalar states $\tilde{t}_L$, $\tilde{t}_R$ is postulated. The two scalar states mix to form mass eigenstates $\tilde{t}_1$, $\tilde{t}_2$, where, by convention, $\tilde{t}_1$ is the lightest. Because of the large top quark Yukawa coupling, large stop masses tend to introduce large fine tuning [7, 8] in many supersymmetric models (and notably in the MSSM [9, 10]). Naturalness requirements normally set upper bounds for stop masses in the TeV range (although recent re-analyses of the fine tuning concept led to relax these requirements significantly [11]). These bounds may imply that the stops are within energetic reach of the LHC. This has triggered a lot of interest by the LHC collaborations (see, for example, Refs. [12–16]). Tight constraints have been set by both the ATLAS and CMS collaborations in many simplified and more realistic supersymmetric models.

This work aims to extend the analysis described in Ref. [17] and develop an event selection yielding optimal sensitivity to stop pair production with 3 ab^{-1} of proton-proton collisions, expected to be collected by ATLAS by the end of the HL-LHC run. R-parity is assumed to be conserved [18]. The only supersymmetric particles assumed to have impact on the stop decay are the stop itself and the lightest supersymmetric particle (LSP), assumed to be a neutralino. With these assumptions, the stop decay is $\tilde{t}_1 \to t^{(*)}\tilde{\chi}_1^0$, where the star indicates that the top quark can possibly be off mass-shell, depending on the mass difference between the stop and the neutralino masses, $\Delta m(\tilde{t}_1, \tilde{\chi}_1^0)$. The final state considered is that where both top quarks decay hadronically: it is hence characterised by the presence of many jets and b-jets, and by missing transverse momentum $\mathbf{p}_T^{\text{miss}}$ (whose magnitude will be indicated by E_T^{miss} in the following) stemming from the presence of the two $\tilde{\chi}_1^0$. The process is illustrated in Figure 1.

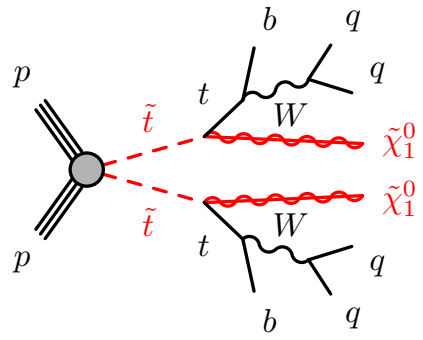

Figure 1: Signal processes considered in this analysis. The top quark can be either on or off mass-shell.

Two kinematic regimes are considered:

- If the difference between the stop and neutralino masses is large with respect to the top quark mass $\Delta m(\tilde{t}_1, \tilde{\chi}_1^0) \gg m_{\text{top}}$, then the top quarks emitted in the stop decay are produced on shell, and they have a boost in the laboratory frame proportional to $\Delta m(\tilde{t}_1, \tilde{\chi}_1^0)$. The final state is hence characterised by high p_T jets and b-jets, and large E_T^{miss}. Typical analyses in this kinematic regimes have large signal acceptance, and the sensitivity is limited by the signal cross section, that decreases steeply

with increasing $m\left(\tilde{t}_1\right)$. The sensitivity to 3 ab^{-1} of proton-proton collisions in this kinematic regime was already studied in Ref. [19]. This regime is the target of the "large Δm" analysis described in this document.

- If $\Delta m(\tilde{t}_1, \tilde{\chi}_1^0) \sim m_{\text{top}}$, then the extraction of the signal from the Standard Model (SM) background stemming from mainly $t\bar{t}$ production requires a focus on events where the stop pair system recoils against substantial initial-state hadronic activity (ISR). The upgrade sensitivity to this scenario has never been investigated before by ATLAS in final states with no leptons (see Ref. [20] for a study in final states with two leptons). It is the target of the "diagonal" analysis described in this document.

2 The ATLAS Detector

The predicted response of the ATLAS during HL-LHC is emulated by a set of smearing functions applied on top of the final-state particles, defined as those with a lifetime larger than $\tau = 30$ ps. A description of the emulation of the upgraded ATLAS detector is given in Ref. [21]. The smearing functions have been determined from a full GEANT 4 [22] simulation of the upgraded ATLAS detector [23] assuming an average number of additional collisions per bunch-crossing $\langle\mu\rangle = 200$.

3 Event Simulation

The analysis is performed on datasets of SM background processes and supersymmetric signals simulated through different event generators. Signal models are all generated assuming a proton-proton collision centre-of-mass energy $\sqrt{s} = 14$ TeV with MADGRAPH5_aMC@NLO 2.2–2.4 [24] interfaced to PYTHIA 8 [25] for the parton showering (PS) and hadronisation and with EVTGEN 1.2.0 [26] for the b- and c-hadron decays. The matrix element (ME) calculation is performed at tree level and includes the emission of up to two additional partons for all signal samples. In case of top quark off-shell decay, the MadSpin routine is used to preserve the correct spin correlations and phase space modelling. The parton distribution function (PDF) set used for the generation of the signal samples is NNPDF2.3LO [27] with the A14 [28] set of tuned underlying-event and shower parameters (UE tune). The ME–PS matching was performed with the CKKW-L [29] prescription, with a matching scale set to one quarter of the mass of the $\tilde{t}_1$. All signal cross sections were calculated at next-to-leading order in the strong coupling constant, adding the resummation of soft-gluon emission at next-to-leading-logarithm accuracy (NLO+NLL) [30–32]. They strongly depend on the stop mass: for example, the stop pair production cross section is 12.9 (0.14) fb for a stop mass of 900 (1600) GeV.

SM background samples were produced with different MC event generators depending on the process. The background sources of Z + jets and W+ jets events were generated with SHERPA 2.2.1 [33] using the NNPDF3.0NNLO [27] PDF set and the UE tune provided by SHERPA. Top-quark pair production where at least one of the top quarks decays semileptonically and single-top production were simulated with POWHEG-BOX 2 [34] and interfaced to PYTHIA 8 for PS and hadronization, with the CT10 [35] PDF set and using the PERUGIA2012 [36] set of tuned shower and underlying-event parameters. MADGRAPH5_aMC@NLO interfaced to PYTHIA 8 for PS and hadronization was used to generate the $t\bar{t}+V$ (where V is a W or Z boson) samples at NLO with the NNPDF3.0NLO PDF set. The underlying-event tune used is A14 with the NNPDF2.3LO PDF set. Additional information can be found in Refs. [37–40]

Z + jets, W+ jets, $t\bar{t}+V$, diboson and single top $s-$ and $t-$channel production events are all simulated assuming $\sqrt{s} = 13$ TeV, and an event weight is assigned according to the ratio between the relevant PDF distributions to emulate $\sqrt{s} = 14$ TeV events. Wt and $t\bar{t}$ production events are generated directly assuming a centre-of-mass energy $\sqrt{s} = 14$ TeV. The samples are normalised to the $\sqrt{s} = 14$ TeV cross section at NNLO (for $t\bar{t}$ [41]) and NLO (for Wt [42]). The values used are $\sigma_{t\bar{t}} = 984.5$ pb and $\sigma_{Wt} = 84.4$ pb.

4 Final State Object Definition

The event selection is based on variables constructed from the kinematics of particle-level objects, selected according to reconstruction-level quantities obtained from the emulation of the detector response for HL-LHC [21].

Electrons are defined with a `Loose` identification criterion with $p_{\mathrm{T}} > 7$ GeV and $|\eta| < 2.47$. Muons are defined with a `Loose` identification criterion, and are required to have $p_{\mathrm{T}} > 6$ GeV and $|\eta| < 2.7$. Baseline anti-k_t $R = 0.4$ jets [43, 44] are required to have $p_{\mathrm{T}} > 20$ GeV and $|\eta| < 2.8$[1]. Jets arising from the fragmentation of b-hadrons are tagged with a nominal efficiency of 70%, computed on a $t\bar{t}$ sample simulated assuming $\langle\mu\rangle$. The corresponding rejection factor for jets originating from the fragmentation of a c (light) quark is about 20 (750) [45]. Ambiguities between the reconstruction of leptons and jets are resolved following the same overlap-removal procedure outlined in Ref. [17].

Reclustered jets are created by applying the anti-k_t algorithm with distance parameters $\Delta R = 0.8$ and $\Delta R = 1.2$ on signal jets, indicated in the following as anti-$k_t^{0.8}$ and anti-$k_t^{1.2}$ jet collections. A trimming procedure [46] is applied that removes $R = 0.4$ jets from the reclustered jets if their p_{T} is less than 5% of the p_{T} of the anti-$k_t^{0.8}$ or anti-$k_t^{1.2}$ jet p_{T}.

5 Event Selection

Two different event selections are developed. They respectively target the signal parameter space where $\Delta m(\tilde{t}_1, \tilde{\chi}_1^0) \gg m_{\mathrm{top}}$ or $\Delta m(\tilde{t}_1, \tilde{\chi}_1^0) \sim m_{\mathrm{top}}$. They will be referred to as the "large Δm" and "diagonal" analyses respectively. In both cases, the selection follows closely that developed for the analysis of the dataset collected in 2015 and 2016, published in Ref. [17]: the same set of selection variables is used, although the thresholds are in some case modified to account for the higher integrated luminosity and the higher level of noise induced by pileup collisions at the HL-LHC.

5.1 Large Δm Selection

The variables used in Ref. [17] for the event selection in the signal regions targeting large $\Delta m(\tilde{t}_1, \tilde{\chi}_1^0)$ are here briefly summarised:

- N_{lep}**:** The total number of baseline leptons in the event after overlap removal.

[1] Although the upgraded ATLAS detector will allow to efficiently suppress pileup up to large pseudorapidity, the final state objects produced by stop pair production tend to be central: it has been verified that increasing the pseudorapidity of the jet selection does not affect the final result of the analysis.

- $\boldsymbol{N_{\text{jet}}}$**:** The total number of signal jets.
- $\boldsymbol{N_{b-\text{jet}}}$**:** The total number of b-jets.
- $\boldsymbol{p_{\text{T}}^{\text{jet}i}}$**:** The p_{T} of the i-th anti-$k_t^{0.4}$ jet (where the ordering is done in p_{T}). The leading jet is labelled with $i = 1$.
- $\boldsymbol{m_i^{\text{anti-}k_t^R}}$**:** The mass of the i-th (ordering done in mass) reclustered anti-k_t jet reconstructed with distance parameter R. The leading jet is labelled with $i = 1$.
- $\boldsymbol{m_{\text{Tb}}^{\text{min}}}$**:** The transverse mass m_{T}[2] between the $\mathbf{p}_{\text{T}}^{\text{miss}}$ and the b-jet with the minimum $\Delta\phi$ to the $\mathbf{p}_{\text{T}}^{\text{miss}}$. This variable is known to have a kinematical end-point at the top quark mass for SM $t\bar{t}$ production.
- $\boldsymbol{\Delta R_{bb}}$**:** The ΔR distance between the two b-jets in the event. If more than two b-jets are present, those with the highest p_{T} are considered.
- $\boldsymbol{m_{\text{T}}^{\chi^2}}$**:** Stransverse mass computed using the $\mathbf{p}_{\text{T}}^{\text{miss}}$ and the transverse momenta of the top candidates. They are defined by minimising (among all possible candidates) a χ^2:

$$\chi^2 = \frac{\left(m_W^{\text{cand1}} - m_W^{\text{truth}}\right)^2}{m_W^{\text{truth}}} + \frac{\left(m_W^{\text{cand2}} - m_W^{\text{truth}}\right)^2}{m_W^{\text{truth}}} + \frac{\left(m_{\text{top}}^{\text{cand1}} - m_{\text{top}}^{\text{truth}}\right)^2}{m_{\text{top}}^{\text{truth}}} + \frac{\left(m_{\text{top}}^{\text{cand2}} - m_{\text{top}}^{\text{truth}}\right)^2}{m_{\text{top}}^{\text{truth}}}.$$

  The candidates W are constructed using all possible combinations of one and two non-b-tagged jets. If more than two b-jets are present, the two with the highest p_{T} are considered.

A preselection is applied, which is summarised in Table 1. A lepton veto and a selection on the number of jets characterise the choice of focusing on fully hadronic events. The selection on $\Delta\phi\left(E_{\text{T}}^{\text{miss}}, \text{jet}^{1,2}\right)$ is known to be extremely effective in suppressing multijet production events, where the $\mathbf{p}_{\text{T}}^{\text{miss}}$ vector tends to be aligned with one of the jets. The selection on $E_{\text{T}}^{\text{miss}}$ exploits the presence of the non-interacting neutralinos in the final state. The selections on the anti-$k_t^{1.2}$ and anti-$k_t^{0.8}$ jet masses exploit the potential presence of boosted top quarks and W-bosons in the final state. The selection on $m_{\text{Tb}}^{\text{min}}$ is effective in suppressing events from SM $t\bar{t}$ production.

For the evaluation of the final exclusion sensitivity, a set of mutually exclusive signal regions is defined. The background after preselection is dominated by $t\bar{t}$ and single top Wt production. For both of these processes, the largest contribution comes from events where one of the two W bosons decays hadronically and the other decays leptonically (there including $W \to \tau\nu$). The dominant background processes hence feature at most one hadronic top and/or W decay, while the signal features two of them. The events are hence further classified in 30 different signal regions according to the number of identified b-jets, the value of $m_2^{\text{anti-}k_t^{1.2}}$ mass, and the value of the $E_{\text{T}}^{\text{miss}}$. In each $N_{b-\text{jet}}$ bin, three bins are defined in $m_2^{\text{anti-}k_t^{1.2}}$. In order, it corresponds to having found a jet with mass: i) below that of the W boson, ii) similar to that of the W boson, iii) loosely consistent with that of the top quark. Finally, in each bin a set of $E_{\text{T}}^{\text{miss}}$ intervals are defined. In the bin with $N_{b-\text{jet}} \geq 2$, there is no ambiguity[3] in the definition of the two expected b-jets

[2] The transverse mass between two vectors in the transverse plane **a** and **b** forming an angle θ between them is defined as $m_{\text{T}} = \sqrt{2ab\,(1 - \cos\theta)}$.

[3] If $N_{b-\text{jet}} > 2$ then the two b-jets with the highest p_{T} are used.

Table 1: Selection applied for the large Δm analysis.

Preselection	
$N_{\text{lep}} = 0$	
$N_{\text{jet}} \geq 4$	
$\Delta\phi\left(E_{\text{T}}^{\text{miss}}, \text{jet1}\right) > 0.4$, $\Delta\phi\left(E_{\text{T}}^{\text{miss}}, \text{jet2}\right) > 0.4$	
$N_{b-\text{jet}} \geq 1$	
$E_{\text{T}}^{\text{miss}} > 400$ GeV	
$p_{\text{T}}^{\text{jet1}} > 80$ GeV, $p_{\text{T}}^{\text{jet2}} > 80$ GeV	
$p_{\text{T}}^{\text{jet3}} > 40$ GeV, $p_{\text{T}}^{\text{jet4}} > 40$ GeV	
$m_1^{\text{anti-}k_t^{1.2}} > 120$ GeV	
$m_{\text{Tb}}^{\text{min}} > 250$ GeV	
$m_1^{\text{anti-}k_t^{0.8}} > 60$ GeV, $m_2^{\text{anti-}k_t^{0.8}} > 60$ GeV	
Signal region selection	
Number of b-tagged jets	Other selections
$N_{b-\text{jet}} = 1$	$m_2^{\text{anti-}k_t^{1.2}} \in [0, 60), [60, 120), [120, \infty)$ $E_{\text{T}}^{\text{miss}} \in [400, 600), [600, 900), [900, 1200), [1200, 1600), [1600, \infty)$
$N_{b-\text{jet}} > 1$	$m_2^{\text{anti-}k_t^{1.2}} \in [0, 60), [60, 120), [120, \infty)$ $E_{\text{T}}^{\text{miss}} \in [400, 600), [600, 900), [900, 1200), [1200, 1600), [1600, \infty)$ $m_{\text{T}}^{\chi^2} > 400$, $\Delta R_{bb} \geq 1$

from the stop decay, thus the $m_{\text{T}}^{\chi^2}$ and ΔR_{bb} are well defined. Additional selections on these variables are therefore applied. The full set of signal region selections is also presented in Table 1.

The $E_{\text{T}}^{\text{miss}}$ distributions for $N_{b-\text{jet}} \geq 2$ and for the two tightest bins in $m_2^{\text{anti-}k_t^{1.2}}$, that is, for the two bins that are most sensitive for large $\Delta m(\tilde{t}_1, \tilde{\chi}_1^0)$ values, are shown in Figure 2.

For the evaluation of the discovery sensitivity, a set of single bin cut-and-count signal regions is defined, which apply the full preselection, and then require $N_{b-\text{jet}} \geq 2, m_2^{\text{anti-}k_t^{1.2}} > 120\,\text{GeV}$. Four different thresholds in $E_{\text{T}}^{\text{miss}}$ are then defined to achieve optimal sensitivity for a 5σ discovery: $E_{\text{T}}^{\text{miss}} > 400, 600, 800, 1000$ GeV. For each model considered, the signal region giving the lowest p-value against the background-only hypothesis in presence of the signal is used.

To avoid depending too much on the limited size of the background samples generated for this study, the background $E_{\text{T}}^{\text{miss}}$ distribution is parametrised independently for each $N_{b-\text{jet}}$, $m_2^{\text{anti-}k_t^{1.2}}$ bin and for each process with a simple exponential function. The function parameters are determined by fitting it to the MC predicted distribution in the range $E_{\text{T}}^{\text{miss}} > 400$ GeV.

5.2 Diagonal Selection

The selection for the region of the signal parameter space where $\Delta m(\tilde{t}_1, \tilde{\chi}_1^0) \sim m_{\text{top}}$ also follows closely that developed in Ref. [17]. The basic idea of the diagonal analysis arise from the fact that, given the mass relation between the stop and the neutralino, the stop decay products (the top quark and the neutralino) are produced nearly at rest in the stop reference frame. When looked at from the lab reference frame, the

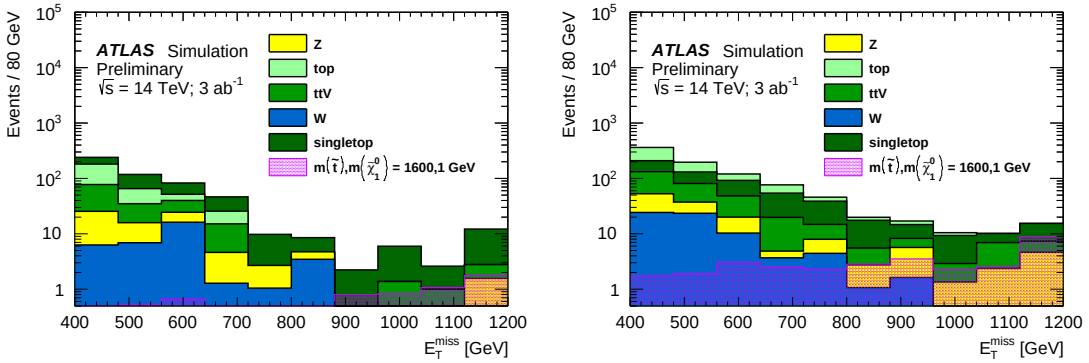

(a) $N_{b-\text{jet}} \geq 2$, 60 GeV $< m_2^{\text{anti-}k_t^{1.2}} \leq$ 120 GeV (b) $N_{b-\text{jet}} \geq 2$, $m_2^{\text{anti-}k_t^{1.2}} >$ 120 GeV

Figure 2: The $E_{\text{T}}^{\text{miss}}$ distributions for the two bins with the highest sensitivity to signals with large values of $\Delta m(\tilde{t}_1, \tilde{\chi}_1^0)$. The last bin includes overflow events.

transverse momentum acquired by the decay products will be proportional to their mass. If $p_{\text{T}}^{\text{ISR}}$ is the transverse momentum of everything that recoils against the stop pair, it can be shown that [47]

$$R_{\text{ISR}} = \frac{E_{\text{T}}^{\text{miss}}}{p_{\text{T}}^{\text{ISR}}} \sim \frac{m\left(\tilde{\chi}_1^0\right)}{m\left(\tilde{t}_1\right)} \tag{1}$$

Following this considerations, a recursive jigsaw [48] reconstruction is performed, which makes assumptions that allow the definition of a set of variables in different reference frames. In this specific case, it first defines the centre-of-mass of the primary proton-proton collision, or **CM** frame. In the **CM** frame, the sparticles frame **S** and the ISR system (**ISR**) are back-to-back to each other. One can then define the Visible (**V**) and Invisible (**I**) reference frames, composed respectively by the visible particles produced in the stop pair decay and the invisible particles produced in the stop pair decay. New variables are defined to exploit the relation suggested by Equation 1.

The following variables are used specifically for the diagonal analysis.

- $\boldsymbol{p_{\text{T}}^{\text{ISR}}}$ The total momentum of the **ISR** system in the **CM** frame.
- $\boldsymbol{R_{\text{ISR}}}$ This is defined as the ratio of the projection of total momentum of the invisible system in the **CM** frame on the total momentum of the **ISR** frame in the **CM** frame, to the the total momentum of the **ISR** frame in the **CM** frame. That is

$$R_{\text{ISR}} = \frac{|\vec{p}_{\mathbf{I}}^{\mathbf{CM}} \cdot \hat{p}_{\mathbf{ISR}}^{\mathbf{CM}}|}{|\vec{p}_{\mathbf{ISR}}^{\mathbf{CM}}|} \tag{2}$$

- $\boldsymbol{N_{b-\text{jet}}^{\text{S}}}$ The number of b-jets assigned to the frame **V**.
- $\boldsymbol{N_{\text{jet}}^{\text{S}}}$ The number of jets assigned to the frame **V**.
- $\boldsymbol{p_{\text{T}}^{4,\text{S}}}$ The transverse momentum of the 4th jet associated with the **V** frame.

- $\boldsymbol{\Delta\phi(\text{ISR}, \mathbf{p}_{\text{T}}^{\text{miss}})}$ The distance in azimuthal angle between the **ISR** and **I** total momentum vectors in the **CM** frame.
- $\boldsymbol{m_{\text{S}}}$ The mass of the **S** frame.
- $\boldsymbol{p_{\text{T},b}^{0,\text{S}}}$ The transverse momentum of the leading b-jet associated to the **V** frame.

The preselection applied for the diagonal analysis is summarised in Table 2.

Figure 3 shows the distribution of some of the key variables after the selection on $p_{\text{T}}^{4,\text{S}}$. The main features which were observed in Ref. [17] are still present: the m_{S} variable peaks at roughly twice the top mass for the signal, the position of the peak of the R_{ISR} variable increases with the ratio $m\left(\tilde{\chi}_1^0\right)/m\left(\tilde{t}_1\right)$, there is a strong peak at π for the signal for $\Delta\phi(\text{ISR}, \mathbf{p}_{\text{T}}^{\text{miss}})$. Already at this stage of the selection, the main background process is $t\bar{t}$.

Table 2: Selection applied for the diagonal analysis.

Preselection	
$N_{\text{lep}} = 0$	
$N_{\text{jet}} \geq 4$	
$\Delta\phi\left(E_{\text{T}}^{\text{miss}}, \text{jet1}\right) > 0.4, \Delta\phi\left(E_{\text{T}}^{\text{miss}}, \text{jet2}\right) > 0.4$	
$N_{b-\text{jet}} \geq 1$	
$E_{\text{T}}^{\text{miss}} > 400$ GeV	
$p_{\text{T}}^{\text{jet1}} > 80$ GeV, $p_{\text{T}}^{\text{jet2}} > 80$ GeV	
$p_{\text{T}}^{\text{jet3}} > 40$ GeV, $p_{\text{T}}^{\text{jet4}} > 40$ GeV	
$N_{b-\text{jet}}^{\text{S}} \geq 1$	
$N_{\text{jet}}^{\text{S}} \geq 5$	
$p_{\text{T},b}^{0,\text{S}} > 40$ GeV	
$m_{\text{S}} > 300$ GeV	
$\Delta\phi(\text{ISR}, \mathbf{p}_{\text{T}}^{\text{miss}}) > 3$	
$p_{\text{T}}^{\text{ISR}} > 400$ GeV	
$p_{\text{T}}^{4,\text{S}} > 50$ GeV	
Signal region selection	
R_{ISR} selection	$E_{\text{T}}^{\text{miss}}$ selection
$0.5 < R_{\text{ISR}} < 0.65$	$E_{\text{T}}^{\text{miss}} \in [500, 700), [700, 1000), [1000, 1400), [1400, \infty)$
$R_{\text{ISR}} > 0.65$	$E_{\text{T}}^{\text{miss}} \in [500, 700), [700, 1000), [1000, 1400), [1400, \infty)$

A possible strategy is suggested by figure 3(d): the $E_{\text{T}}^{\text{miss}}$ distribution shifts progressively higher values of $m\left(\tilde{t}_1\right)$. Hence a boost in sensitivity could be obtained by binning the signal regions in this variable. The final strategy for the assessment of exclusion sensitivity for the diagonal analysis is thus to use a set of mutually exclusive signal region defined in bins of R_{ISR} and $E_{\text{T}}^{\text{miss}}$. The final binning is shown in Table 2. Lower values of R_{ISR} are not considered given that the current analysis focuses mostly on the prospects for high $m\left(\tilde{t}\right)$. For the evaluation of the discovery sensitivity, four cut-and-count signal regions are defined, which apply the full preselection, and then require $R_{\text{ISR}} > 0.7$ and $E_{\text{T}}^{\text{miss}} > 500, 700, 900, 1100$ GeV. For each model considered, the signal region giving the lowest p-value against the SM hypothesis in presence of signal is used.

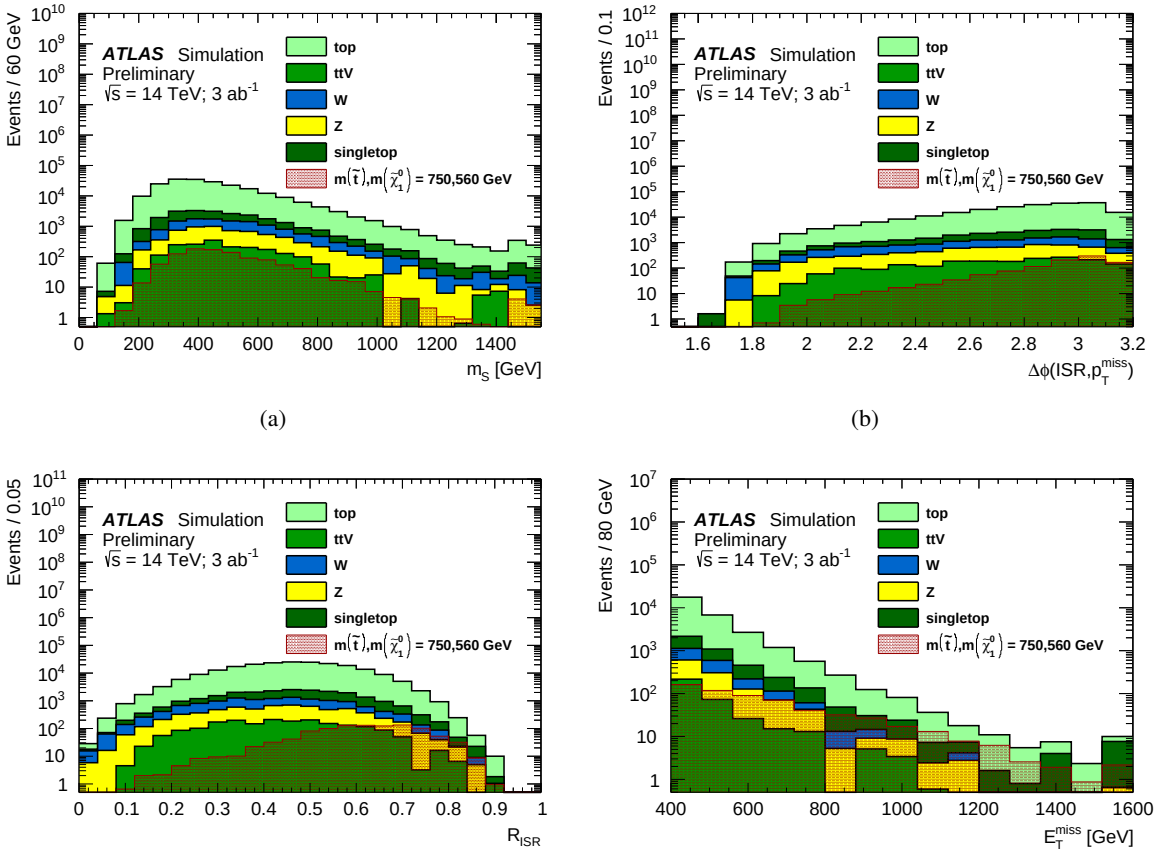

(a) (b) (c) (d)

Figure 3: Distributions of the main variables of the diagonal selection, after all cuts up to that on $p_{\mathrm{T}}^{4,\mathrm{S}}$ have been applied. The signal and backgrounds are normalised to 3 ab^{-1}. The last bin includes overflow events.

Similarly to the large Δm analysis, the background estimation used for the assessment of the analysis sensitivity stems from a parameterisation of the actual background MC. The background is parametrised in $E_{\mathrm{T}}^{\mathrm{miss}}$ in each bin of R_{ISR} and independently for each background process. The parametrisation is established for $E_{\mathrm{T}}^{\mathrm{miss}} > 500$ GeV, and it is done with a simple exponential function.

6 Systematic Uncertainties

Realistic and pessimistic uncertainty scenarios have been determined starting from the systematic uncertainties studied in Ref. [17], and extrapolating them to 3 ab^{-1} following a common approach agreed upon by the ATLAS and CMS collaborations. Hence, the theory modelling uncertainties are expected to be reduced by a factor 2, while different recommendations have been provided for detector-level and experimental uncertainties.

With reference to Ref. [17]:

- For the large Δm analysis, the total systematic uncertainty in the signal regions that targeted the same parameter space region as this analysis was evaluated to be 14–24%. The dominant uncertainties were due to jet energy scale (JES - 7%) and resolution (JER - 5–10%), $t\bar{t}$ and Wt parton shower and generator uncertainties (5–12%). Owing to the reduced statistical uncertainty and a better understanding of the physics models, it is expected that JES, JER and top modelling uncertainties will all be reduced. It is assumed that they will all be halved by the end of the HL-LHC running. This leads to an estimate of the uncertainty for the large Δm analysis of about 15% or less, depending on the phase space region. Given how relevant the Wt background process is, special care will be needed to make sure that the treatment of interference terms between $t\bar{t}$ and Wt and the corresponding uncertainty will be under control by the end of the HL-LHC.
- For the diagonal analysis, the estimated uncertainties in Ref. [17] were about 20%, with the exception of one region that was affected by large statistical uncertainty in the MC samples for $t\bar{t}$. The dominant uncertainty in all cases was connected with the modelling of ISR in $t\bar{t}$ events. For the uncertainty projection, it was decided to proceed as for the case of the large Δm uncertainty to halve the $t\bar{t}$ modelling uncertainties. The result is a predicted uncertainty of 17% for the tightest R_{ISR} bin.

In conclusion, a 15% uncertainty is retained as a baseline value of the expected uncertainty for both the large Δm and the diagonal analysis to determine both the 5σ and the 95% CL exclusion reach of the analysis. For the case of the estimation of the 95% CL exclusion sensitivity, a further scenario with doubled uncertainty (30%) is also evaluated.

7 Results

The final $E_{\mathrm{T}}^{\mathrm{miss}}$ distribution in the bins with $m_2^{\text{anti-}k_t^{1.2}} > 120$ GeV, $N_{b-\mathrm{jet}} \geq 2$ (for the large Δm analysis) and $R_{\mathrm{ISR}} > 0.65$ (for the diagonal analysis) are shown in Figure 4.

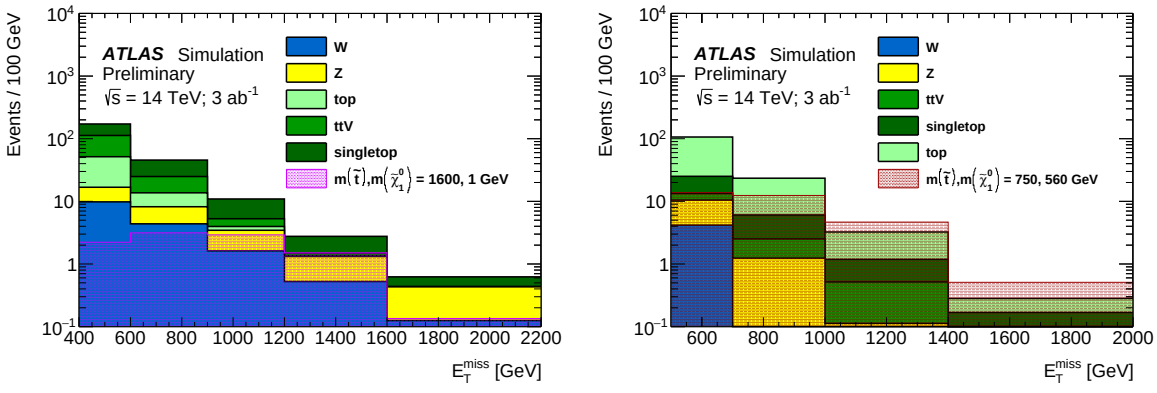

(a) (b)

Figure 4: $E_{\mathrm{T}}^{\mathrm{miss}}$ distribution for (a) the $m_2^{\text{anti-}k_t^{1.2}} > 120$ GeV, $N_{b-\mathrm{jet}} \geq 2$ bin of the large Δm analysis and (b) $R_{\mathrm{ISR}} > 0.65$ bin of the diagonal analysis. The last bin includes overflow events.

The final exclusion sensitivity evaluation is done by performing a profile-likelihood fit to a set of pseudo-data providing bin-by-bin yields corresponding to the background expectations. For each of the two

analyses (large Δm and diagonal), the likelihood is built as the product of poissonian terms, one for each of the considered bins. Systematic uncertainties are accounted for by introducing one independent nuisance parameter for each of the bins considered. The likelihood is modified introducing gaussian terms representing the assumed uncertainty. 95% CL exclusion contours on the masses of the supersymmetric particles are extracted using the CLs method [49]. For each mass of the stop and the neutralino, the analysis yielding the smallest CLs among the large Δm and the diagonal is used.

The discovery sensitivity is obtained similarly from each of the single cut-and-count regions independently. For each signal point, the profile likelihood ratio fit is performed on pseudo-data corresponding to the sum of the expected background and the signal. The discovery contour corresponds to points expected to give a 5σ p-value against the background-only hypothesis. For each signal point, the discovery signal region yielding the smallest p-value is considered.

The final sensitivity of the analysis is summarised in Figure 5 assuming a 15% uncertainty for the 5σ discovery and 95% CL exclusion contour, and also assuming 30% uncertainty for the 95% CL exclusion contour.

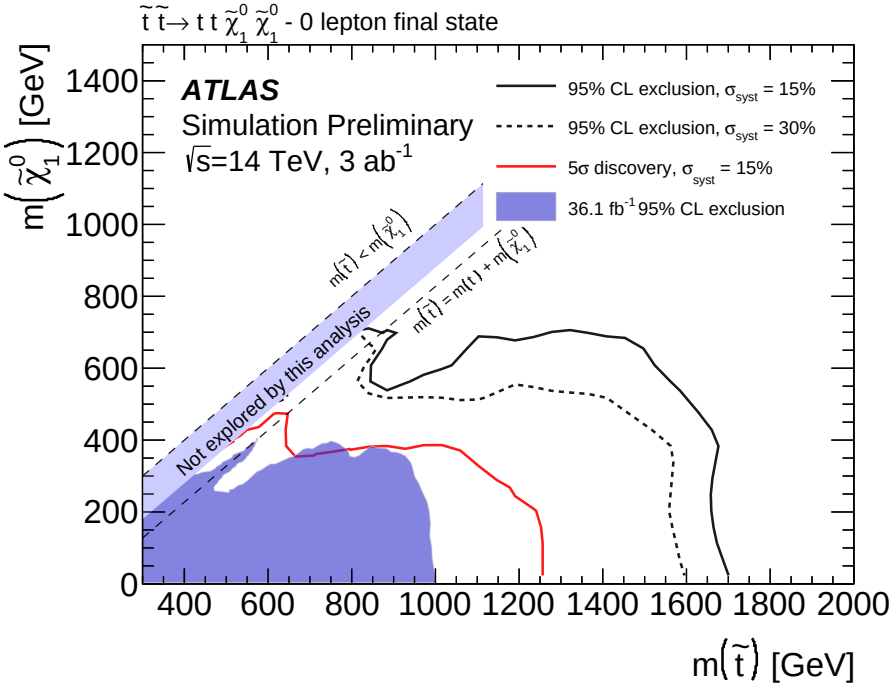

Figure 5: Final 95% CL exclusion reach and 5σ discovery contour corresponding to 3 ab^{-1} of proton-proton collisions collected by ATLAS at the HL-LHC.

8 Conclusions

The ATLAS sensitivity to stop pair production with 3 ab^{-1} of proton-proton collisions and running conditions corresponding to those of the HL-LHC is estimated with an analysis that follows closely that published in Ref. [17]. The process of interest is $\tilde{t}_1 \rightarrow t^{(*)}\tilde{\chi}_1^0$. Event containing no leptons are retained, and

two separate selections are developed targeting regions of the parameter space where $\Delta m(\tilde{t}_1, \tilde{\chi}_1^0) \gg m_{\text{top}}$ or $\Delta m(\tilde{t}_1, \tilde{\chi}_1^0) \sim m_{\text{top}}$. 95% CL exclusion and 5σ discovery contours are derived in the $\left(m\left(\tilde{t}_1\right), m\left(\tilde{\chi}_1^0\right)\right)$ plane for uncertainty assumptions which are either realistic or pessimistic extrapolations of the current uncertainties. Stops can be discovered (excluded) up to masses of 1.25 (1.7) TeV for $m\left(\tilde{\chi}_1^0\right) \sim 0$ under realistic uncertainty assumptions. The reach in stop mass degrades for larger neutralino masses. If $\Delta m(\tilde{t}_1, \tilde{\chi}_1^0) \sim m_{\text{top}}$, then the discovery (exclusion) reach is 650 (850) GeV.

References

[1] Yu. A. Golfand and E. P. Likhtman,
Extension of the Algebra of Poincare Group Generators and Violation of p Invariance,
JETP Lett. **13** (1971) 323, [Pisma Zh. Eksp. Teor. Fiz. **13** (1971) 452].

[2] D. V. Volkov and V. P. Akulov, *Is the Neutrino a Goldstone Particle?*, Phys. Lett. B **46** (1973) 109.

[3] J. Wess and B. Zumino, *Supergauge Transformations in Four-Dimensions*,
Nucl. Phys. B **70** (1974) 39.

[4] J. Wess and B. Zumino, *Supergauge Invariant Extension of Quantum Electrodynamics*,
Nucl. Phys. B **78** (1974) 1.

[5] S. Ferrara and B. Zumino, *Supergauge Invariant Yang-Mills Theories*, Nucl. Phys. B **79** (1974) 413.

[6] A. Salam and J. A. Strathdee, *Supersymmetry and Nonabelian Gauges*, Phys. Lett. B **51** (1974) 353.

[7] R. Barbieri and G. F. Giudice, *Upper Bounds on Supersymmetric Particle Masses*,
Nucl. Phys. B **306** (1988) 63.

[8] B. de Carlos and J. A. Casas, *One loop analysis of the electroweak breaking in supersymmetric models and the fine tuning problem*, Phys. Lett. B **309** (1993) 320, arXiv: hep-ph/9303291.

[9] P. Fayet, *Supersymmetry and Weak, Electromagnetic and Strong Interactions*,
Phys. Lett. B **64** (1976) 159.

[10] P. Fayet,
Spontaneously Broken Supersymmetric Theories of Weak, Electromagnetic and Strong Interactions,
Phys. Lett. B **69** (1977) 489.

[11] H. Baer, V. Barger, M. Savoy, and X. Tata,
Multi-channel assault on natural supersymmetry at the high luminosity LHC,
Phys. Rev. D **94** (2016) 1, arXiv: 1604.07438 [hep-ph].

[12] ATLAS Collaboration, *ATLAS Run 1 searches for direct pair production of third-generation squarks at the Large Hadron Collider*, Eur. Phys. J. C **75** (2015) 510,
arXiv: 1506.08616 [hep-ex].

[13] ATLAS Collaboration,
Search for top-squark pair production in final states with one lepton, jets, and missing transverse momentum using 36 fb^{-1} of $\sqrt{s}$ = 13 TeV pp collision data with the ATLAS detector,
JHEP **06** (2018) 108, arXiv: 1711.11520 [hep-ex].

[14] CMS Collaboration,
Search for third-generation leptoquarks and scalar bottom quarks in pp collisions at $\sqrt{s}$ = 7 TeV,
JHEP **12** (2012) 055, arXiv: 1210.5627 [hep-ex].

[15] CMS Collaboration,
Search for supersymmetry in proton–proton collisions at 13 *TeV using identified top quarks*,
Phys. Rev. D **97** (2018) 012007, arXiv: 1710.11188 [hep-ex].

[16] CMS Collaboration, *Search for direct production of supersymmetric partners of the top quark in the all-jets final state in proton–proton collisions at* $\sqrt{s}$ = 13 *TeV*, JHEP **10** (2017) 005,
arXiv: 1707.03316 [hep-ex].

[17] ATLAS Collaboration, *Search for a scalar partner of the top quark in the jets plus missing transverse momentum final state at* $\sqrt{s}$ = 13 *TeV with the ATLAS detector*, JHEP **12** (2017) 085,
arXiv: 1709.04183 [hep-ex].

[18] G. R. Farrar and P. Fayet, *Phenomenology of the Production, Decay, and Detection of New Hadronic States Associated with Supersymmetry*, Phys. Lett. B **76** (1978) 575.

[19] ATLAS Collaboration, *Prospects for benchmark Supersymmetry searches at the high luminosity LHC with the ATLAS Detector*, ATL-PHYS-PUB-2013-011, 2013,
URL: https://cds.cern.ch/record/1604505.

[20] ATLAS Collaboration, *Prospects for a search for direct pair production of top squarks in scenarios with compressed mass spectra at the high luminosity LHC with the ATLAS Detector*,
ATL-PHYS-PUB-2016-022, 2016, URL: https://cds.cern.ch/record/2220904.

[21] ATLAS Collaboration, *Expected performance of the ATLAS detector at the HL-LHC*, In progress, 2018.

[22] S. Agostinelli et al., *GEANT4–a simulation toolkit*, Nucl. Instrum. Meth. A **506** (2003) 250.

[23] ATLAS Collaboration, *The ATLAS Simulation Infrastructure*, Eur. Phys. J. C **70** (2010) 823,
arXiv: 1005.4568 [physics.ins-det].

[24] J. Alwall et al., *The automated computation of tree-level and next-to-leading order differential cross sections, and their matching to parton shower simulations*, JHEP **07** (2014) 079,
arXiv: 1405.0301 [hep-ph].

[25] T. Sjöstrand, S. Mrenna, and P. Z. Skands, *A brief introduction to PYTHIA 8.1*,
Comput. Phys. Commun. **178** (2008) 852, arXiv: 0710.3820 [hep-ph].

[26] D. J. Lange, *The EvtGen particle decay simulation package*, Nucl. Instrum. Meth. **462** (2001) 152.

[27] R. D. Ball et al., *Parton distributions with LHC data*, Nucl. Phys. B **867** (2013) 244,
arXiv: 1207.1303 [hep-ph].

[28] ATLAS Collaboration, *ATLAS Run 1 Pythia8 tunes*, ATL-PHYS-PUB-2014-021, 2014,
URL: https://cds.cern.ch/record/1966419.

[29] L. Lönnblad and S. Prestel, *Merging multi-leg NLO matrix elements with parton showers*,
JHEP **03** (2013) 166, arXiv: 1211.7278 [hep-ph].

[30] W. Beenakker, M. Kramer, T. Plehn, M. Spira, and P. M. Zerwas,
Stop production at hadron colliders, Nucl. Phys. B **515** (1998) 3, arXiv: hep-ph/9710451.

[31] W. Beenakker et al., *Supersymmetric top and bottom squark production at hadron colliders*,
JHEP **08** (2010) 098, arXiv: 1006.4771 [hep-ph].

[32] W. Beenakker, S. Brensing, M. Kramer, A. Kulesza, E. Laenen, et al.,
Squark and gluino hadroproduction, Int. J. Mod. Phys. A **26** (2011) 2637,
arXiv: 1105.1110 [hep-ph].

[33] T. Gleisberg et al., *Event generation with SHERPA 1.1*, JHEP **02** (2009) 007, arXiv: 0811.4622 [hep-ph].

[34] S. Alioli, P. Nason, C. Oleari, and E. Re, *A general framework for implementing NLO calculations in shower Monte Carlo programs: the POWHEG BOX*, JHEP **06** (2010) 043, arXiv: 1002.2581 [hep-ph].

[35] H.-L. Lai et al., *New parton distributions for collider physics*, Phys. Rev. D **82** (2010) 074024, arXiv: 1007.2241 [hep-ph].

[36] P. Z. Skands, *Tuning Monte Carlo generators: the Perugia tunes*, Phys. Rev. D **82** (2010) 074018, arXiv: 1005.3457 [hep-ph].

[37] ATLAS Collaboration, *Monte Carlo Generators for the Production of a W or Z/γ^* Boson in Association with Jets at ATLAS in Run 2*, ATL-PHYS-PUB-2016-003, 2016, URL: https://cds.cern.ch/record/2120133.

[38] ATLAS Collaboration, *Multi-Boson Simulation for 13 TeV ATLAS Analyses*, ATL-PHYS-PUB-2016-002, 2016, URL: https://cds.cern.ch/record/2119986.

[39] ATLAS Collaboration, *Modelling of the $t\bar{t}H$ and $t\bar{t}V$ ($V = W, Z$) processes for $\sqrt{s} = 13$ TeV ATLAS analyses*, ATL-PHYS-PUB-2016-005, 2016, URL: https://cds.cern.ch/record/2120826.

[40] ATLAS Collaboration, *Validation of Monte Carlo event generators in the ATLAS Collaboration for LHC Run 2*, ATL-PHYS-PUB-2016-001, 2016, URL: https://cds.cern.ch/record/2119984.

[41] LHC physics working group, *NNLO+NNLL top-quark-pair cross sections*, https://twiki.cern.ch/twiki/bin/view/LHCPhysics/TtbarNNLO, [Online; accessed 13-August-2018], 2018.

[42] LHC physics working group, *NLO single-top channel cross sections*, https://twiki.cern.ch/twiki/bin/view/LHCPhysics/SingleTopRefXsec, [Online; accessed 13-August-2018], 2018.

[43] M. Cacciari, G. P. Salam, and G. Soyez, *The anti-k_t jet clustering algorithm*, JHEP **04** (2008) 063, arXiv: 0802.1189 [hep-ph].

[44] M. Cacciari, G. P. Salam, and G. Soyez, *FastJet User Manual*, Eur. Phys. J. C **72** (2012) 1896, arXiv: 1111.6097 [hep-ph].

[45] ATLAS Collaboration, *Technical Design Report for the ATLAS Inner Tracker Pixel Detector*, ATLAS-TDR-030, 2017, URL: http://cdsweb.cern.ch/record/2285585.

[46] ATLAS Collaboration, *Performance of jet substructure techniques for large-R jets in proton–proton collisions at $\sqrt{s} = 7$ TeV using the ATLAS detector*, JHEP **09** (2013) 076, arXiv: 1306.4945 [hep-ex].

[47] H. Wan and L.T. Wang, *Opening up the compressed region of top squark searches at 13 TeV LHC*, Phys. Rev. Lett. **115** (2015) 181602, arXiv: 1506.00653 [hep-ph].

[48] P. Jackson and C. Rogan, *Recursive jigsaw reconstruction: HEP event analysis in the presence of kinematic and combinatoric ambiguities*, Phys. Rev. D **96** (11 2017) 112007, arXiv: 1705.10733 [hep-ph].

[49] S. L. Read, *Presentation of search results: the CL_s technique*, J. Phys. G **28** (2002) 2693.